

Article

The Potential Application of MnZn Ferrite Nanofluids for Wettability Alteration and Oil-Water Interfacial Tension Reduction

Nurul Afiqah Mohd Mokhtar, Hoe Guan Beh * and Kean Chuan Lee 

Fundamental and Applied Sciences Department, Universiti Teknologi PETRONAS, Seri Iskandar 32610, Perak, Malaysia; fieqamokhtar@gmail.com (N.A.M.M.); lee.kc@utp.edu.my (K.C.L.)

* Correspondence: beh.hoeguan@utp.edu.my; Tel.: +60-5368-7699

Received: 18 October 2019; Accepted: 25 November 2019; Published: 27 November 2019



Abstract: Recently, a non-invasive method of injecting magnetic/dielectric nanofluids into the oil reservoir was used for oil recovery application. The use of magnetic nanofluids in Enhanced Oil Recovery (EOR) has been reported to improve oil recovery. It is believed that the magnetic properties of nanoparticles (NPs) have a direct influence on the viscosity and wettability of nanofluid, and on oil-water interfacial tension (IFT). Thus, $Mn_{0.5}Zn_{0.5}Fe_2O_4$ (MnZn) ferrites may be a good candidate to be used in nanofluids for wettability alteration and oil-water IFT reduction due to their excellent magnetic properties, such as a high initial permeability and low magnetic losses. Therefore, this work investigated the potential of MnZn ferrite NPs to alter viscosity, wettability, and oil-water IFT. MnZn Ferrite NPs have been synthesized by a sol-gel auto-combustion process. The effects of calcination temperature varying from 300 °C to 700 °C on the phase formation, microstructures such as surface morphology, and magnetic characterizations were studied. MnZn ferrite nanofluids were prepared using synthesized MnZn NPs that dispersed into brine along with sodium dodecylbenzenesulfonate (SDBS) as a dispersant, and their effects on the wettability and oil-water IFT were studied. X-ray diffraction (XRD) measurements revealed that MnZn ferrite calcined at 300 °C and 400 °C were single phase. The average crystallite size calculated through Scherrer's equation differed from 32.0 to 87.96 nm. The results showed that the nanofluid with MnZn particles calcined at 300 °C is the best nanofluid in terms of IFT reduction and base nanofluid's wettability alteration. Moreover, the overall results proved that nanofluid with MnZn ferrite NPs can alter the wettability of base nanofluid, oil-nanofluid IFT, and nanofluid viscosity. This study provides insights towards a better understanding of the potential application of MnZn Ferrite nanofluids to Wettability Alteration and IFT Reduction in Enhanced Oil Recovery.

Keywords: Ferrite; Nanoparticles; Nanofluid; Contact Angle

1. Introduction

Various techniques were implemented to increase the amount of crude oil extracted from an oil field, and it is strongly believed that Enhanced Oil Recovery (EOR) technology can accommodate future energy demand [1,2]. The EOR technique needs to be used because the conventional methods (primary and secondary recovery) are undesirable and inefficient for removing the massive amount of remaining oil in the reservoirs [3]. Nanotechnology plays a large role in helping the new emerging technologies to overcome the many limitations of thermal, miscible, and other types of recovery methods [4–6]. The contribution to the recovery of oil by Nanoparticles (NPs) is due to the reduction in the interfacial tension between wetting fluid and oil and the increase in viscosity of the displacing fluid that causes greater oil recovery [7,8].

Some NPs such as zinc oxide (ZnO), aluminum oxide (Al₂O₃), zirconium dioxide (ZrO₂), and silicon oxide (SiO₂) have proven their ability as efficient EOR agents for interfacial tension (IFT) reduction [9–12]. Ogolo et al. [6] studied the usefulness of magnetic/dielectric NPs (ZnO, Al₂O₃, NiO, SiO₂ and MgO) in different base fluids including brine, distilled ethanol, and distilled water for EOR. They found that the Al₂O₃ dispersed in distilled water and brine has a tendency to improve oil recovery by causing a reduction in oil viscosity. However, SiO₂ in ethanol improves oil recovery through a wettability alteration. Recently, a non-invasive method of injecting magnetic/dielectric nanofluids into the oil reservoir simultaneously with electromagnetic (EM) irradiation was used for oil recovery applications [13]. Hassan et al. [13] proposed a novel EOR method using Co²⁺_xFe²⁺_{1-x}Fe³⁺₂O₄ as magnetic NPs activated by EM Waves. They concluded that there was a more than 20% increase in oil recovery with Co²⁺_xFe²⁺_{1-x}Fe³⁺₂O₄ nanofluids under the application of EM waves. It was reported that the oil droplets surrounded by NPs are deformed by an external field [14]. The magnetic nanofluid has the capability to interact with a magnetic field. In the presence of a magnetic field, the particles inside the nanofluid will react, thus affecting it by increasing the viscosity of the displacing fluid, which leads to a higher sweep efficiency [15]. The magnetic nanofluid also can reduce the resistance of the crude oil inside the reservoir. This is due to the presence of a dipole moment, which resulted in the alignment of the reservoir fluid, thus reducing the resistance. The presence of magnetic nanoparticles in surfactant can change the IFT value of surfactant/oil interface to make it more effective. Therefore, MnZn ferrite may be a suitable magnetic NP for IFT alteration due to its excellent magnetic properties. The crystal structure of Mn-Zn ferrites is a typical spinel structure with the chemical formula of AB₂O₄. This kind of crystal structure is made up of 64 tetrahedral sites (A-site) and 32 octahedral sites (B-site) in each unit cell interstitial, which are occupied by ions of different elements [16]. In a typical Mn-Zn ferrite crystal structure, zinc ions inhabit the A-sites while the ions of iron and manganese are spread over both A-sites and B-sites. A substituting metal ion with the ionic charge of 3+ would either diffuse properly into the crystal lattice and replace the Fe³⁺ within the crystal structure, or would independently form secondary compounds and aggregate at the grain boundaries, depending on the type of substituting ion and synthesis parameters (calcination temperature, pH, etc.). The proper diffusion of substituting ions into the crystal lattice will alter the otherwise normal spin exchange between the Fe³⁺ ions. Although the use of EM-assisted magnetic nanofluids in EOR has been reported to improve oil recovery, the influence of EM-assisted MnZn magnetic nanofluids on the viscosity, wettability, and oil-water IFT was not widely reported. Therefore, this research work was conducted to determine the potential of MnZn ferrite NPs under the influence of EM to alter the viscosity, wettability, and oil-water IFT.

2. Materials and Methods

2.1. Materials

In this experiment, the reagents used include manganese (II) nitrate tetrahydrate (Mn(NO₃)₂·4H₂O), zinc nitrate (Zn(NO₃)₂·6H₂O), iron (III), nitrate (Fe(NO₃)₂·9H₂O), citric acid (C₆H₈O₇), and ammonia solution for the synthesis of the materials. Calcium chloride (CaCl₂), magnesium chloride (MgCl₂), potassium chloride (KCl), strontium chloride (SrCl₂), sodium chloride (NaCl), barium chloride (BaCl₂), sodium carbonate (NaHCO₃), and sodium sulphate (Na₂SO₄) were used for the preparation of synthetic seawater. All of these reagents were purchased from Sigma-Aldrich and used without further purification, while deionized water was used throughout the experiment.

2.2. Nanoparticles Synthesis

Mn_{0.5}Zn_{0.5}Fe₂O₄ (MnZn ferrite) particles were synthesized through a sol-gel auto-combustion method. The precursor materials, manganese nitrate Mn(NO₃)₂·4H₂O, zinc nitrate Zn(NO₃)₂·6H₂O, iron nitrate Fe(NO₃)₃·9H₂O, and citric acid (C₆H₈O₇·H₂O) were of analytical grade and were readily used without further purification. The molar ratio of metal nitrates to citric acid was kept at 1:2. The metal nitrates were dissolved separately in distilled water before being mixed together, followed by the addition of citric acid solution. Ammonia solution was slowly added to the mixture to bring the pH to 7. The

mixed solution was left to stir with heating at 80 °C on the hot plate until it formed a viscous and thick gel. With an increased heating temperature, water was evaporated, and the mixture began to froth. After a few minutes, the gel ignited and burned in a self-propagating manner to form brown colored ashes. The resultant product was crushed and was calcined at temperatures between 300 °C to 700 °C and was then ready to be used for the nanofluid preparation. The as-prepared MnZn ferrite nanoparticles, with varying calcination temperatures were then characterized using X-ray diffraction (XRD), a field emission scanning electron microscope (FESEM), and a vibrating sample magnetometer (VSM).

2.3. XRD, FESEM & VSM Characterizations

The synthesized powders were characterized through XRD analysis by using a Bruker D8 powder diffraction system equipped with Cu-K α radiation source ($\lambda = 1.5418 \text{ \AA}$), at scanning angles between 20° and 80°. Meanwhile, the studies of the surface morphology were investigated using FESEM. Magnetic properties such as the magnetic saturation, M_s , and coercivity, H_c , of the samples were characterized by using VSM (Lakeshore 7400 Series VSM). The samples were driven to saturation by an applied field of 1.5 T at room temperature.

2.4. Nanofluids Preparation

The MnZn Ferrite nanofluids were prepared using as-prepared MnZn ferrite NPs synthesized at different calcination temperatures (300 °C–700 °C). The stabilizer used in this experiment was SDBS. The appropriate amount of SDBS was dispersed in synthetic seawater as the base fluid (nanofluid) and magnetically stirred until it formed a homogenous solution. The MnZn ferrite nanoparticles suspensions were further agitated in an ultrasonic bath for 30 minutes to reduce agglomeration and ensure longer dispersion in an aqueous solution.

2.5. Interfacial Tension, Contact Angle and Viscosity Measurements

The sessile drop technique was used to measure the IFT and contact angle of oil/nanofluid and oil/MnZn ferrite nanofluids. These measurements were conducted by using a Rame-Hart (260-F4) goniometer (surface tension accuracy = $\pm 0.01 \text{ mN/m}$, contact angle accuracy = $\pm 0.1^\circ$). The system consisted of a glass cell container, while a glass plate representing sandstone was placed in the glass cell container filled with the nanofluid. The container was surrounded by solenoid coil and connected with an RF generator (Agilent 33500B) to generate EM waves. A small drop of the Tapis crude oil of $24 \pm 0.2 \mu\text{L}$ was placed underneath the glass plate using an inverted syringe. The camera connected to computer was used to magnify and take the images for the DROP. The software DROP image was used to evaluate the IFT(γ) by using the following equation:

$$\gamma = \Delta\rho g R^2 / \beta \quad (1)$$

where γ is surface tension, $\Delta\rho$ is the difference in densities between the oil drop and nanofluid, g is the gravitational constant, R is the radius of the droplet, and β is the shape factor. The contact angle of solid-nanofluid was measured using the DROP image software through image analysis technique. The viscosity of the nanofluid was measured using a Brookfield CAP 2000+Rheometer, with the maximum rotation set to 100 rpm at a room temperature of 25 °C. The IFT, viscosity, and contact angle were measured with the presence of EM waves.

3. Results

3.1. XRD Analysis

The NPs of MnZn Ferrite have successfully been synthesized by a sol-gel auto-combustion process. Structural, morphological, and magnetic properties of MnZn ferrite NPs were investigated for different calcination temperature. The XRD patterns for all five compounds, scanned from 20° to 90°, are shown in Figure 1. The changing intensity of diffraction line in the XRD pattern confirms the polycrystalline

nature of the synthesized ferrite. The peaks with the highest intensity observed in the diffraction patterns, at approximately 35.2° , correspond to the major phase of MnZn ferrite nanocrystal. This, along with the other peaks assigned to the reflection planes (220), (311), (400), (422), (511), (440), and (335), matches well with the standard diffraction peaks of MnZn ferrite (JCPDS (10-0467)) and are denoted as (α -phase). The diffraction patterns for MnZn ferrite samples calcined at 300°C and 400°C matched well to that of spinel manganese ferrite. Based on the XRD pattern produced and on the phase content % calculation done (Table 1), the cubic spinel structure of MnZn ferrite was the dominant phase present in sample calcined at 500°C , with the existence of few additional peaks representing minor secondary phases. The secondary peaks detected were attributed to the phases of ZnFe_2O_4 and MnFe_2O_4 . The major peak at $2\theta = 32.2^\circ$ which corresponded to the formation of MnFe_2O_4 began to become a dominant phase when MnZn Ferrite calcined at 600°C and 700°C .

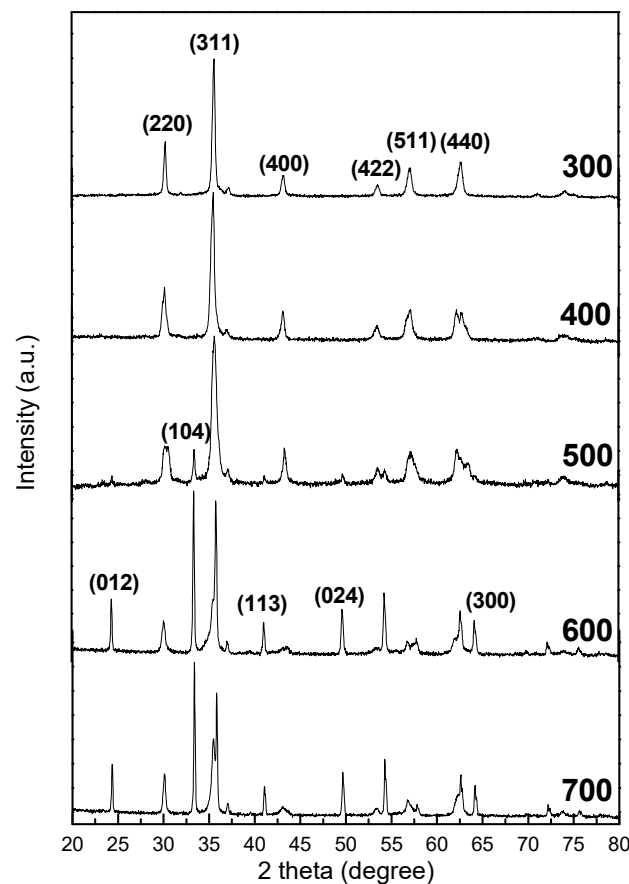


Figure 1. XRD pattern of MnZn Ferrite calcined at various temperatures.

By taking the most outstanding peak which corresponds to the reflection plane (311) for samples calcined at 300°C , 400°C . and 500°C , and the reflection plane (104) for samples calcined at 600°C and 700°C , the interplanar spacing d_{hkl} was calculated using Bragg's equation, which in turn helped to obtain the lattice constant 'a' through the equation:

$$a = d_{hkl} \sqrt{h^2 + k^2 + l^2}$$

where (h, k, l) represented the Miller indices. Separately, the average crystallite size of the samples was calculated from the XRD peak broadening pattern using Scherrer's equation as follows:

$$D = 0.9\lambda/B\cos\theta$$

where D is the average crystallite size, λ is the wavelength of the x-ray source (1.5406 \AA), B is the full width at half maximum (FWHM), and θ is the Bragg's angle. Both calculated values are shown in

Table 1. It was observed that the crystallite size of the MnZn increases at a temperature of 400 °C and decreases at a temperature of 500 °C. This can be attributed to the reduction of the crystallinity and phase content of MnZn ferrite. As can be seen in the Table 1 the phase content of MnZn Ferrite decreased with the increasing of calcination temperature. At a calcination temperature of 600 °C, the crystallite size of the sample increased tremendously. This trend can be attributed to the development of the MnFe_2O_4 phase. The crystallite size of MnZn Ferrite was within the range of 32.0 to 87.96 nm. The lattice constant of MnZn ferrite exhibited a similar trend to the particle size.

Table 1. Lattice constant, D-spacing, crystallite size, and phase content of MnZn Ferrite nanoparticles.

Calcination Temperature (°C)	Lattice Constant, a (Å)	D-Spacing (Å)	Average Crystallite Size (nm)	Phase Content of $\text{MnZnFe}_2\text{O}_4$ (%)	Phase Content of ZnFe_2O_4 (%)	Phase content of MnFe_2O_4 (%)	Phase Content of Fe_2O_3 (%)
300	8.355	2.519	34.2	100	-	-	-
400	8.430	2.542	43.84	100	-	-	-
500	8.369	2.523	32.0	61	36	3	-
600	8.403	2.534	87.96	7	17	44	32
700	8.387	2.529	86.23	11	15	36	38

3.2. FESEM Analysis

The surface morphology of the MnZn Ferrite synthesized at various calcination temperatures were analyzed through FESEM. As shown in Figure 2, the particles were closely packed and irregular in size with the size distributed in a range of 72–150.0 nm. Few pores were observed in between particles in the samples, as shown in Figure 2A–D. Prominent particle agglomeration was observed with each increase in the calcination temperature. The magnetic nanoparticles tended to agglomerate because of their magnetic properties. Moreover, a high calcination temperature led to the agglomeration of particles due to emerging forces including capillary, electrostatic, and Van-der Waals forces which produce mutual interactions between microparticles [17,18].

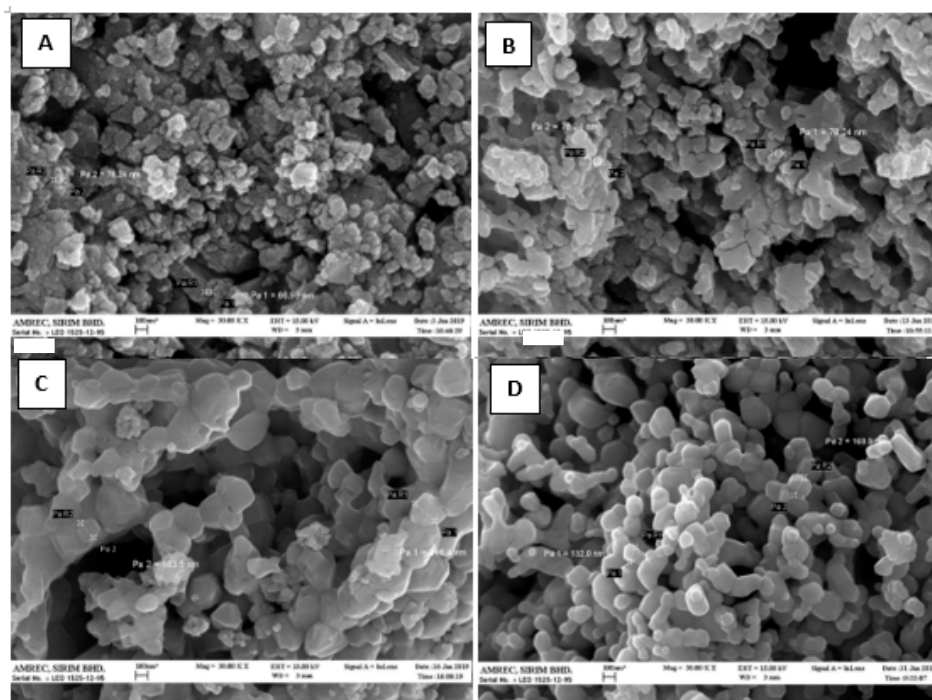


Figure 2. FESEM images of MnZn Ferrite calcined at various temperatures (A) 300 °C (B) 400 °C (C) 500 °C (D) 700 °C with a scale bar of 200 nm.

3.3. VSM Analysis

The magnetic properties of the prepared samples were measured through VSM measurements, with an applied maximum applied field of 15 kOe. The resultant magnetic hysteresis is shown in Figure 3. The dependence of the magnetic parameters such as magnetic saturation, M_s and coercivity, H_c , on the calcination temperature was analyzed using this hysteresis loop. The M_s and H_c values for different calcination temperatures are given in Table 2. As the calcination temperature increased from 400 °C to 600 °C, the saturation magnetization showed a significant decrease due to the decrease in the phase content of $MnZnFe_2O_4$ (Table 1). It could be observed from Figure 3 that the value of saturation magnetization (M_s) for the $MnZnFe_2O_4$ sample calcined at 300 °C was slightly higher than the sample calcined at 400 °C. This may have been due to a high crystallinity and uniform morphologies, which can be observed from Figure 2. The saturation of magnetization decreased tremendously at a calcination temperature of 500 °C, which can be attributed to the development of a $ZnFe_2O_4$ phase (Table 1). The hysteresis curves of $MnZn$ Ferrite calcined at 300 °C and 400 °C show ferromagnetic behavior, however at 500 °C it behaved as a weak ferromagnetic and at 600 °C and 700 °C it acted as an antiferromagnetic. This can be attributed to the reduction of the $MnZn$ Ferrite phase and the development of antiferromagnetic Fe_2O_3 phases in the sample. A coercive field is in the field when M and H change their sign, and one can see from Figure 3 that a small level of coercivity was observed which was assigned to the typical soft ferromagnetic behavior of $MnZn$ Ferrite. The coercivity of $MnZnFe_2O_4$ increased with the increasing of the calcination temperature, which may have been due to the irregular large pores on grain boundaries hindering the domain wall motion. It is well known that coercivity is caused by the resistance of domain wall displacement [12].

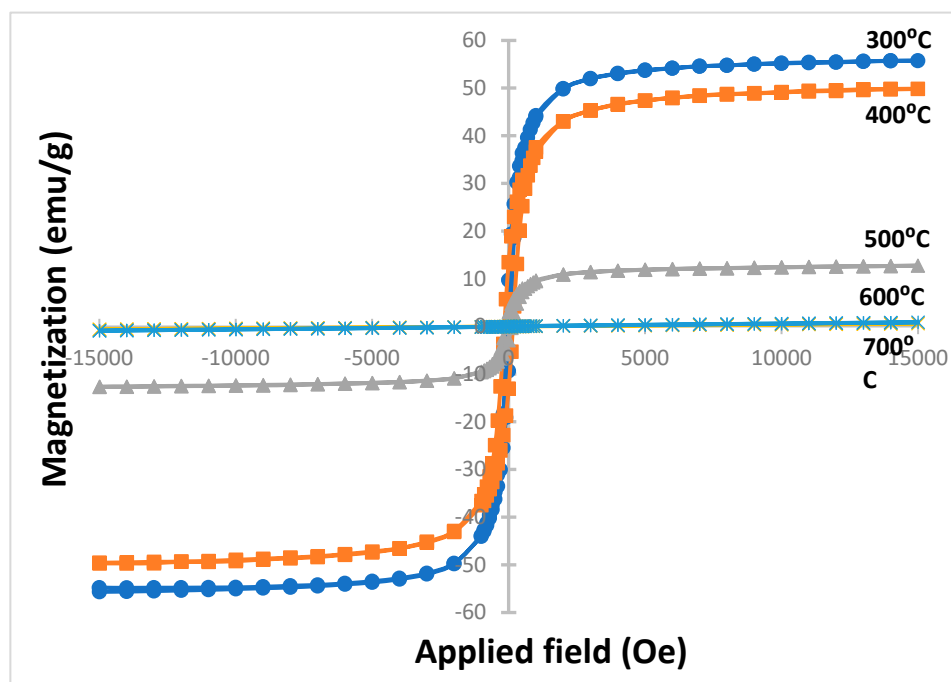


Figure 3. Magnetic hysteresis loops of $MnZn$ Ferrite particles calcined at various temperatures.

Table 2. Magnetic saturation, M_s and coercivity, H_c values at various calcination temperatures.

Calcination Temperature ($^{\circ}\text{C}$)	H_c (Oe)	M_s (emu/g)
300	59.9	55.8
400	156.42	49.8
500	110.95	12.7
600	122.19	0.613
700	129.67	0.878

3.4. IFT Analysis

MnZn ferrite calcined at various temperatures in synthetic seawater solution (nanofluid) was tested for its effects on reducing IFT between nanofluid and crude oil at room temperature. Figure 4 shows the IFT measurement for oil/nanofluids with MnZn Ferrite calcined at various temperatures and oil/nanofluid without MnZn ferrite. Nanofluid with MnZn ferrite calcined at 300 $^{\circ}\text{C}$ had the lowest IFT, whereas at 500 $^{\circ}\text{C}$ it had the highest IFT value. The IFT value increased from 0.33 mN/m to 0.48 mN/m when the calcination temperature increased from 300 $^{\circ}\text{C}$ to 400 $^{\circ}\text{C}$. The increase in IFT value was attributed to the increase in the crystallite size. The IFT result showed an increasing trend with a calcination temperature of up to 500 $^{\circ}\text{C}$, followed by a decreasing trend at 600 $^{\circ}\text{C}$ and then an increasing trend again at 700 $^{\circ}\text{C}$ (Figure 5). This behavior could be attributed to the fluctuation in magnetization of MnZn Ferrite NPs (Table 2) due to the decrease in the ferromagnetic MnZn Ferrite phase and the development of an antiferromagnetic Fe_2O_3 phase in the sample (Figure 3), suggesting that the magnetic properties of MnZn Ferrite NPs contributes to the IFT alteration, which needs further study. The magnetic polarization of NPs causes the oil drops to deform, which increased the surface area and consequently altered the IFT [19]. The IFT value did not show significant changes for different calcination temperatures. However, MnZn nanofluid gave interesting results compared to the previous report [12,13], while the nanofluid without MnZn ferrite NPs had an IFT value of 4.34 mN/m (Figure 4f). This result indicates that MnZn nanofluids have the potential to improve oil recovery by reducing IFT.

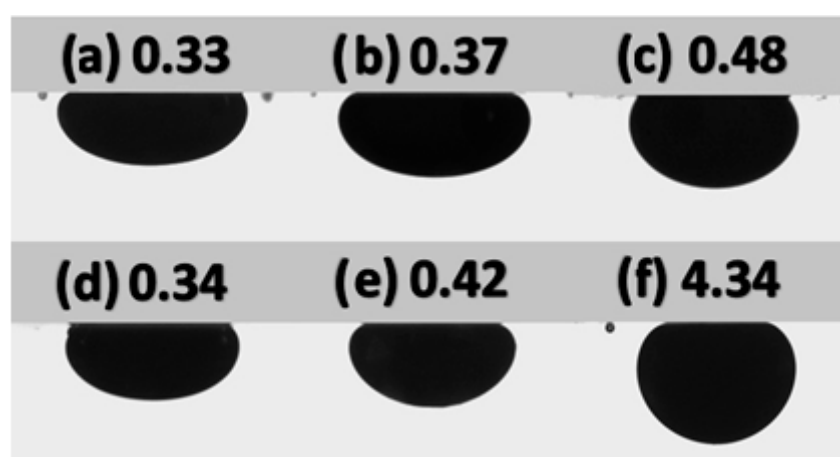


Figure 4. IFT measurement for oil/nanofluids with MnZn Ferrite calcined at temperatures of (a) 300 $^{\circ}\text{C}$, (b) 400 $^{\circ}\text{C}$, (c) 500 v, (d) 600 $^{\circ}\text{C}$, (e) 700 $^{\circ}\text{C}$ and (f) oil/nanofluid (synthetic seawater + SBDS) without MnZn Ferrite.

3.5. Wettability Analysis

Reservoir rock wettability has a massive effect on interface movement and is associated with the displacement of oil through porous media. Oil recovery increases significantly when the wettability of the rock changes from oil-wet to water-wet. Contact angle measurement is an essential enhancing test for wettability alteration study [14,15]. The MnZn ferrite nanofluids were separately dropped on a

glass slide to find their contact angle values. The variation of contact angles on the MnZn Ferrite's calcination temperature is shown in Figure 6. It was observed that the contact angle increases with an increase in the calcination temperature. The increase in contact angle is attributed to the increase in crystallite size and irregular particles in the sample. The findings indicate that the increase of water wetness was due to the decrease in the crystallite size and increases in the regularity of the particle size. In addition, the contact angle of nanofluid without MnZn Ferrite nanoparticles was 48.64° . This value was decreased to a range of 11.97° to 18.93° by introducing an MnZn ferrite nanoparticle in nanofluid. The largest reduction of the contact angle was obtained by MnZn Ferrite calcined at 300°C , while 600°C showed the lowest reduction to a value of 18.93° . Figure 7 shows the measurement of the solid-nanofluid-oil three-phase contact angle. It is observed that the contact angle of oil/MnZn Ferrite nanofluid decreased from 132.5° to 107.0° when the calcination temperature increased from 300°C to 400°C . The contact angle of oil/nanofluid with MnZn ferrite calcined at 300°C has the highest contact angle value, whereas at 400°C it has the lowest contact angle value. Meanwhile, the contact angle of oil/nanofluid with MnZn ferrite calcined at 500°C , 600°C , and 700°C exhibit similar trends to those in IFT measurement (Figure 5).

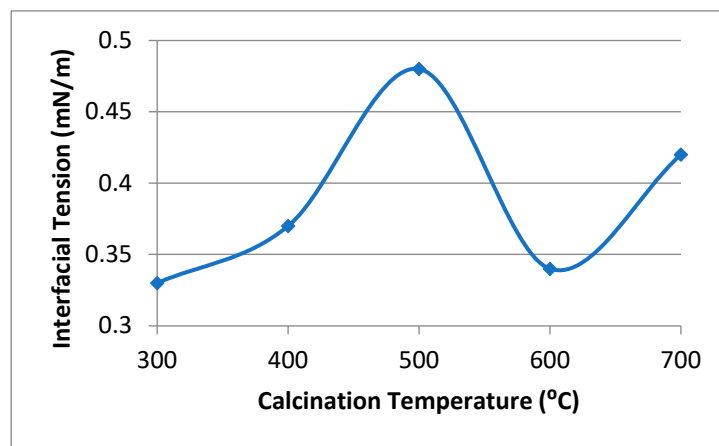


Figure 5. Interfacial tension measurement for oil/nanofluids with MnZn Ferrite calcined at various temperatures.

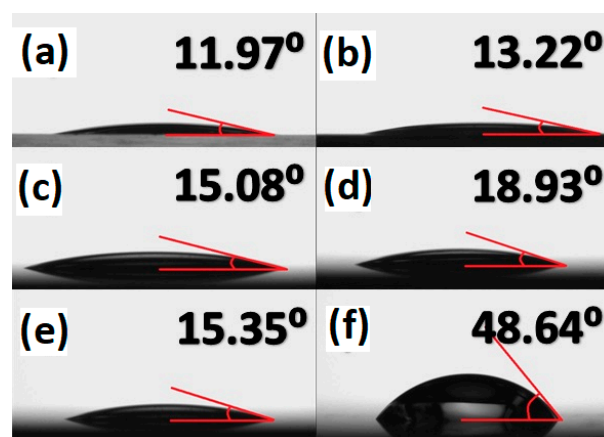


Figure 6. Contact angle measurement for nanofluid with MnZn ferrite nanoparticles calcined at temperature of (a) 300°C , (b) 400°C , (c) 500°C , (d) 600°C , (e) 700°C , and (f) without MnZn Ferrite nanoparticles.

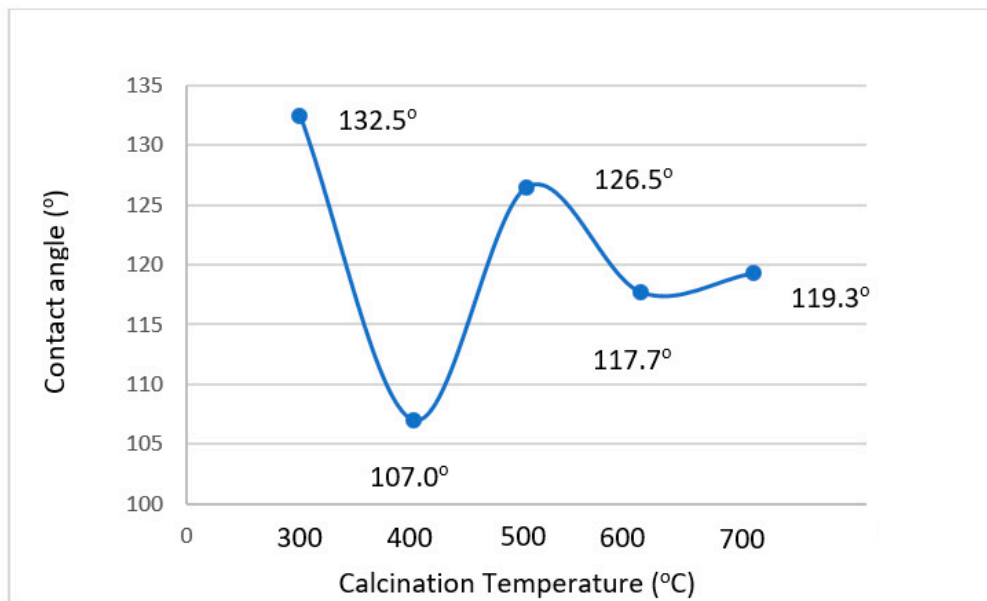


Figure 7. Contact angle measurement for Oil/nanofluid with MnZn ferrite nanoparticles calcined at various temperatures.

3.6. Viscosity Analysis

The viscosity of MnZn Ferrite nanofluids was measured using a Brookfield rheometer DV3T modeled LVTJ0 at 25 °C. The viscosity of these nanofluids was measured with a shear rate from 0 to 122 s⁻¹ and a shear stress of 0.16 Pa. The values reported were the average of the three measurements. Figure 8 shows the effect of calcination temperature on the viscosity of MnZn Nanofluids. It can be seen from Figure 8 that the viscosity increases with the increase in calcination temperature (300 °C to 600 °C). However, it was observed that there was an anomalous reduction of viscosity at temperatures of 500 °C and 700 °C. A similar trend was observed in Figure 2. Therefore, it is suspected that the particles size of MnZn Ferrite was the main factor that contributed to the variation of viscosity. Overall, the viscosity results do not show significant changes with the calcination temperature. It has been reported that a reduction in the oil-water viscosity ratio can improve the oil recovery process because of the formation of oil-water emulsion [20].

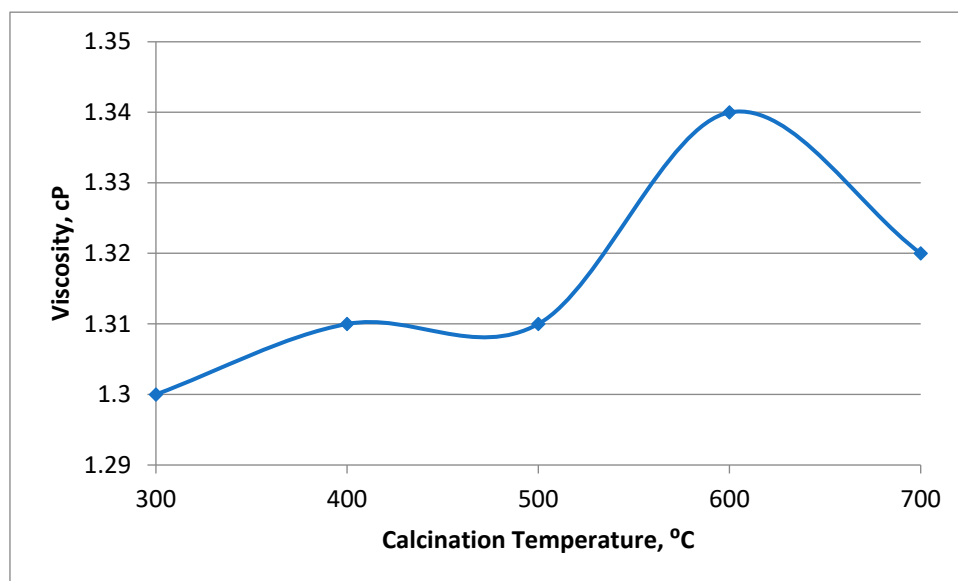


Figure 8. Viscosity for nanofluids with and without MnZn ferrite nanoparticles.

4. Conclusions

Mn-Zn ferrite particles were successfully synthesized at various calcination temperatures through a sol-gel auto-combustion technique. The present study found that the calcination greatly affected the structure, morphology, and magnetic properties of MnZn Ferrite. The surface morphology via FESEM shows particle agglomerations which were irregular in size and with distinct particle shapes. Wettability, IFT, and viscosity results did not show significant changes with the calcination temperature. However, the result showed that introducing the MnZn ferrite nanoparticles in nanofluids significantly altered the wettability of nanofluid and reduced the contact angle between oil and brine on a glass slide. These results suggested that MnZn Ferrite nanoparticles can alter the wettability of nanofluid, oil-nanofluid IFT, and nanofluid viscosity.

Author Contributions: Conceptualization, H.G.B.; Funding acquisition, H.G.B.; Methodology, N.A.M.M.; Project administration, H.G.B.; Writing—original draft, N.A.M.M., H.G.B. and K.C.L.; Writing—review & editing, N.A.M.M. and K.C.L.

Funding: This research was funded by Universiti Teknologi PETRONAS, grant number 015LC0-063 and Universitas Islam Riau (UIR), grant number 015ME0-042.

Acknowledgments: The authors express their appreciation for the financial support of this study by the Yayasan Universiti Teknologi PETRONAS research grant (YUTP Cost Centre: 015LC0-063) and Universitas Islam Riau (UIR) research grant (UIR Cost Centre 015ME0-042). The authors would also like to offer their utmost gratitude to Universiti Teknologi PETRONAS for providing excellent research facilities.

Conflicts of Interest: The authors declare no conflict of interest.

References

1. Alvarado, V.; Manrique, E. Enhanced Oil Recovery: An Update Review. *Energies* **2010**, *3*, 1529–1575. [[CrossRef](#)]
2. Tunio, S.Q.; Tunio, A.H.; Ghirano, N.A.; Adawy, Z.M. Comparison of different enhanced oil recovery techniques for better oil productivity. *Int. J. Appl. Sci. Technol.* **2011**, *1*, 143–153.
3. Yousefvand, H.A.; Jafari, A.; Yousefvand, H.A. Stability and flooding analysis of nanosilica/NaCl/HPAM/SDS solution for enhanced heavy oil recovery. *J. Pet. Sci. Eng.* **2018**, *162*, 283–291. [[CrossRef](#)]
4. Hendraningrat, L.; Li, S.; Torsæter, O. A coreflood investigation of nanofluid enhanced oil recovery. *J. Pet. Sci. Eng.* **2013**, *111*, 128–138. [[CrossRef](#)]
5. Mokhtab, S.; Fresky, M.A.; Islam, M.R. Applications of Nanotechnology in Oil and Gas E&P. *J. Pet. Technol.* **2006**, *58*, 48–51.
6. Ogolo, N.; Olafuyi, O.; Onyekonwu, M. Enhanced Oil Recovery Using Nanoparticles. In *SPE Saudi Arabia Section Technical Symposium and Exhibition*; Society of Petroleum Engineers: Richardson, TX, USA, 2012.
7. Karimi, A.; Fakhroueian, Z.; Bahramian, A.; Pour Khiabani, N.; Darabad, J.B.; Azin, R.; Arya, S. Wettability alteration in Carbonates using zirconium oxide nanofluids: EOR Implications. *Energy Fuels* **2012**, *26*, 1028–1036. [[CrossRef](#)]
8. Esmailnezhad, E.; Le Van, S.; Chon, B.H.; Choi, H.J.; Schaffie, M.; Gholizadeh, M.; Ranjbar, M. An experimental study on enhanced oil recovery utilizing nanoparticle ferrofluid through the application of a magnetic field. *J. Ind. Eng. Chem.* **2018**, *58*, 319–327. [[CrossRef](#)]
9. Esmailzadeh, P.; Hosseinpour, N.; Bahramian, A.; Fakhroueian, Z.; Arya, S. Effect of ZrO₂ Nanoparticles on the interfacial behavior of surfactant solutions at air–water and n-heptane–water interfaces. *Fluid Phase Equilib.* **2014**, *361*, 289–295. [[CrossRef](#)]
10. Zaid, H.M.; Ahmad Latiff, N.R.; Yahya, N. The effect of zinc oxide and aluminum oxide nanoparticles on interfacial tension and viscosity of nanofluids for enhanced oil recovery. *Adv. Mater. Res.* **2014**, *1024*, 56–59. [[CrossRef](#)]
11. Ahmed, A.; Saaid, I.M.; Tunio, A.H.; Pilus, R.M.; Mumtaz, M.; Ahmad, I. Investigation of dispersion stability and IFT reduction using surface modified nanoparticle: Enhanced oil recovery. *J. Appl. Environ. Biol. Sci.* **2017**, *7*, 56–62.
12. Joonaki, E.; Ghanaatian, S. The Application of Nanofluids for Enhanced Oil Recovery: Effects on Interfacial Tension and Coreflooding Process. *Pet. Sci. Technol.* **2014**, *32*, 2599–2607. [[CrossRef](#)]

13. Soleimani, H.; Yahya, N.; Latiff, N.R.A.; Zaid, H.M.; Demiral, B.; Amighian, J. Novel enhanced oil recovery method using $\text{Co}^{2+} x\text{Fe}^{2+}_{1-x} \text{Fe}^{3+}_2 \text{O}_4$ as magnetic nanoparticles activated by electromagnetic waves. *J. Nano Res.* **2014**, *111*–116. [[CrossRef](#)]
14. Cui, M.; Emrick, T.; Russell, T.P. Stabilizing Liquid Drops in Nonequilibrium Shapes by the Interfacial Jamming of Nanoparticles. *Science* **2013**, *342*, 460–463. [[CrossRef](#)] [[PubMed](#)]
15. Kothari, N.; Raina, B.; Chandak, K.B.; Iyer, V.; Mahajan, H.P. *Application of Ferrofluid for Enhanced Surfactant Flooding in Eor*; Society of Petroleum Engineers: Richardson, TX, USA, 2010; p. 131272.
16. Şabikoğlu, I.; Paralı, L.; Malina, O.; Novak, P.; Kaslik, J.; Tuček, J.; Pechousek, J.; Navařík, J.; Schneeweiss, O.; Paralı, L. The effect of neodymium substitution on the structural and magnetic properties of nickel ferrite. *Prog. Nat. Sci.* **2015**, *25*, 215–221. [[CrossRef](#)]
17. Jiang, J.; Yang, Y.-M.; Li, L.-C. Synthesis and magnetic properties of lanthanum-substituted lithium–nickel ferrites via a soft chemistry route. *Phys. B Condens. Matter* **2007**, *399*, 105–108. [[CrossRef](#)]
18. Gaber, A.; Abdel-Rahim, M.; Abdel-Latif, A.; Abdel-Salam, M.N. Influence of calcination temperature on the structure and porosity of nanocrystalline SnO₂ synthesized by a conventional precipitation method. *Int. J. Electrochem. Sci.* **2014**, *9*, 81–95.
19. Adil, M.; Lee, K.C.; Zaid, H.M.; Latiff, N.R.A.; Alnarabiji, M.S. Experimental study on electromagnetic-assisted ZnO nanofluid flooding for enhanced oil recovery (EOR). *PLoS ONE* **2018**, *13*, e0193518. [[CrossRef](#)] [[PubMed](#)]
20. Joonaki, E.; Buckman, J.; Burgass, R.; Tohidi, B. Water versus asphaltenes; liquid-liquid and solid-liquid molecular interactions unravel the mechanisms behind an improved oil recovery methodology. *Sci. Rep.* **2019**, *9*, 1–13. [[CrossRef](#)] [[PubMed](#)]



© 2019 by the authors. Licensee MDPI, Basel, Switzerland. This article is an open access article distributed under the terms and conditions of the Creative Commons Attribution (CC BY) license (<http://creativecommons.org/licenses/by/4.0/>).